Mode coalescence and the Green's function in a two-dimensional waveguide with arbitrary admittance boundary conditions

E. Perrey-Debain*, B. Nennig+, J.B. Lawrie++

*Université de technologie de Compiègne, Roberval (Mechanics, energy and electricity), Centre de recherche Royallieu - CS 60319 - 60203 Compiègne Cedex - France.

+Institut supérieur de mécanique de Paris (ISAE-SUPMECA), Laboratoire Quartz EA 7393, 3 rue Fernand Hainaut, 93407 Saint-Ouen, France.

++Department of Mathematics, Brunel University London, Uxbridge, UB8 3PH.

Abstract

This study focuses on sound attenuation in a two-dimensional waveguide with arbitrary admittance boundary conditions on both sides of the guide. The emphasis is on understanding the formation and potential applications of the exceptional points (EPs) which arise when two (EP2) or three (EP3) modes degenerate into a single mode. A perturbation approach is used to obtain asymptotic expressions for the trajectories of the axial wavenumbers in the complex plane as they coalesce to form an EP. The numerical results presented herein suggest that the first triple root (EP3) assures maximum modal attenuation along the waveguide. Further, it is demonstrated that the classical Green's function is degenerate at an EP. Modified Green's functions which are valid at EP2 and EP3 are presented.

Keywords: Duct acoustics, guided waves, exceptional point, Puiseux series, Green's function, Non-Hermitian physics

1. Introduction

In his seminal article [1], Tester considered sound attenuation in a duct with one rigid wall and one lined. He built upon the work of Cremer [2] who showed that the optimum attenuation within such a duct occurs when a mode pair degenerates into a single mode (an exceptional point). Tester derived the Green's function for this situation and showed that computed results for the attenuation compared favourably with experimental data. In the same decade, Zorumski [3] extended Tester's analysis to the cases of circular ducts with locally reacting liners and Koch [4] used a generalised Wiener-Hopf approach to

study attenuation in a duct with different sections of lining (on both walls). Surprisingly, it took many years before the concept of 'optimal impedance' became a subject of intensive research. Recently, however, interest in the topic has burgeoned and a number of papers have appeared in the literature. Most of these research works deal with circular and annular ducts with flow and have potential application to noise suppression within ducts in aero-engines, gas turbines, blowers and various mufflers [5, 6, 7, 8, 9, 10]. Additionally, [12, 14] consider mode-matching for finite lined region, [13] examines the relationship between the the nature of the source and the transmitted power whilst [11] discusses the form of the additional wavefunctions required at an exceptional point. More recently, the present authors have proposed a numerical algorithm which enables them to explore the trajectories of the eigenvalues in the vicinity of an exceptional point in a systematic way [15]. Despite the recent progress a rigorous description of the mode coalescence, the associated wavefunctions and the modified the Green's functions is still missing from the literature. With the view both to extending the work of Tester and filling this gap, the present study focuses on sound attenuation in a two-dimensional waveguide with arbitrary admittance boundary conditions on both sides of the guide.

In section 2 the boundary value problem is stated and the wave functions associated with mode coalescence are introduced. The analysis starts with the classical solution method which involves expanding the solution in terms of normal modes of separable form: $Y(s,\mu,y)e^{\mathrm{i}sx-\mathrm{i}\omega t}$ where s is the axial wavenumber and $\omega = ck$ in which c is the fluid sound speed and k the wavenumber. For convenience and to aid future manipulations, the lower wall admittance μ is included as a variable in the transverse wavefunction. As usual the precise form of $Y(s,\mu,y)$ is obtained by solving a non-Hermitian eigenvalue problem [16] in which the dispersion relation is even in the transverse wavenumber $\alpha = (k^2-s^2)^{1/2}$. It is well known, however, that there are values of the duct wall admittance(s) for which this approach breaks down due to the existence of non-separable solutions associated with multiple-roots of the dispersion equation [1, 3, 11, 14]. These roots correspond to the coalescence of two (EP2) or three (EP3) acoustic modes and special care must be taken to derive the corresponding waveform. It is shown that the location of EPs in the complex-plane can be described as a function of the product of the two admittances, and the notation $\bar{\alpha}$ is used to denote the transverse wavenumber in this situation. The asymptotic forms (first presented by Tester [1] and Koch [4]) for the value of $\bar{\alpha}$ in the case of one lined and one rigid wall are stated and compared with precise numerical values. A mapping of the complex $\bar{\alpha}$ plane is presented for the fully lined situation.

Section three presents an analysis of the behaviour of the roots coaelescing in the vicinity of an optimal point (ie. when wave attenuation is maximized). The lower wall admittance ($\bar{\mu}$) is kept fixed whilst the wavenumber s and the upper wall admittance are perturbed from their EP values. A double Taylor series is used to expand the dispersion relation and this is then inverted using a Puiseux series. This approach enables the trajectories of the coalescing roots to be plotted in the complex plane for both EP2 and EP3. The link with Cremer's optimum impedance [2] based on the axial attenuation rate is established. It is also shown that there are situations where the acoustic field can exhibit a linear amplification along the waveguide axis with no dissipation at all, that is with purely real axial wavenumber. Further, the numerical results presented herein suggest that the first EP3 (resulting from the coalescence of the first three modes) provides maximum attenuation along the waveguide.

Although interest in exceptional points (EPs) has recently arisen in a variety of physical situations [17, 18, 19, 20], the Green's function for a lined duct at an EP has not, as far as the authors are aware, appeared in the literature except for the case of one hard wall investigated by Tester. This deficiency is addressed in section four where an analysis of the Green's function is presented for EP2 and EP3 using the same methods as in section three. It is demonstrated that the results of Tester are retrieved for the hard wall case. The main results of this article are summarised in section five, together with a brief discussion of their implications for noise control and some suggestions for further work.

2. Analysis of the dispersion equation

Using the usual two-dimensional Cartesian frame of reference, we consider a two-dimensional duct of unit width and local boundary conditions:

$$\partial_y \psi = -\mu\psi, \text{ at } y = 0 \quad \text{and} \quad \partial_y \psi = \nu\psi, \text{ at } y = 1, \tag{1}$$

where μ, ν are the wall admittances. Note that harmonic time dependence $\mathrm{e}^{-\mathrm{i}\omega t}$ is assumed and thus $\psi(x, y)$ is the reduced fluid velocity potential. Solutions of the Helmholtz equation

$$(\partial_{xx}^2 + \partial_{yy}^2 + k^2)\psi = 0, \tag{2}$$

have the general separable form $\psi = Y(s, \mu, y)\,\mathrm{e}^{\mathrm{i}sx}$ where

$$Y(s, \mu, y) = \cos(\alpha y) - \frac{\mu}{\alpha}\sin(\alpha y) \quad \text{with} \quad \alpha = \sqrt{k^2 - s^2}. \tag{3}$$

On using the second condition of Eq. (1), it is clear that

$$(\nu\psi - \partial_y\psi)_{y=1} = K\,\mathrm{e}^{\mathrm{i}sx}, \tag{4}$$

where function K is interpreted as a function of s, μ and ν and is defined by

$$K(s,\mu,\nu) = (\nu+\mu)\,\cos\alpha + \left(\alpha - \frac{\nu\mu}{\alpha}\right)\sin\alpha. \tag{5}$$

Thus, ψ is a solution provided α is a root of the dispersion equation

$$K(s,\mu,\nu) = 0. \tag{6}$$

Note that, whilst α depends on both μ and ν, it is not directly dependent on frequency. Also, it should be observed that functions K and Y are both holomorphic with respect to all their arguments. Because these are even functions of α, they are also holomorphic in s and, when necessary, we can apply the chain rule $\partial_s \equiv -s/\alpha\,\partial_\alpha$. Now, by differentiation, we can define a new wave function

$$\psi' = \partial_s\psi = (Y' + \mathrm{i}xY)\mathrm{e}^{\mathrm{i}sx} \tag{7}$$

with

$$Y' = \partial_s Y = \frac{sy\sin(\alpha y)}{\alpha} + \frac{s\mu y\cos(\alpha y)}{\alpha^2} - \frac{s\mu\sin(\alpha y)}{\alpha^3} \tag{8}$$

and it is easy to see that

$$\partial_s(\nu\psi - \partial_y\psi)_{y=1} = (\nu\psi' - \partial_y\psi')_{y=1} = (K' + \mathrm{i}xK)\mathrm{e}^{\mathrm{i}sx}. \tag{9}$$

Thus ψ' (which is not of separable form) is also solution if the double root problem $K = 0$ and $K' = \partial_s K = 0$ is satisfied. In this case, after some manipulation, we arrive at the set of equations

$$\bar{p} = \bar{\mu}\bar{\nu} = \bar{\alpha}^2\left(\frac{2\bar{\alpha}+\sin(2\bar{\alpha})}{2\bar{\alpha}-\sin(2\bar{\alpha})}\right) \quad \text{and} \quad \bar{q} = \bar{\mu}+\bar{\nu} = -\tan\bar{\alpha}\left(\bar{\alpha} - \frac{\bar{p}}{\bar{\alpha}}\right). \tag{10}$$

Wall parameters which are associated with an exceptional point of order 2 (EP2) are recovered via

$$\bar{\mu} = \frac{\bar{q} - \sqrt{\bar{q}^2 - 4\bar{p}}}{2} \quad \text{and} \quad \bar{\nu} = \frac{\bar{q} + \sqrt{\bar{q}^2 - 4\bar{p}}}{2}. \tag{11}$$

Note that $(\bar{\mu},\bar{\nu})$ as defined by Eqs (11) form a continuous set since $\bar{\alpha}$ can be regarded as an arbitrary complex-valued parameter. From Eq. (10), we recognize the two limit cases corresponding to one hard wall condition $\bar{p} = 0$ (where the reader is reminded that $\bar{p}$ is not the pressure) and one pressure release condition $|\bar{p}| \to \infty$, given by the relations

$$2\bar{\alpha} \pm \sin(2\bar{\alpha}) = 0. \tag{12}$$

Approximate solutions have been given independently by Tester and Koch [1, 4] and these are presented here for completeness:

$$2\bar{\alpha}_m \approx \frac{2m+3}{2}\pi - \mathrm{i}\ln((2m+3)\pi) \quad m = 0, 1, 2, \ldots, \tag{13}$$

where m even corresponds to the hard wall condition $\bar{\mu} = 0$ giving $\bar{\nu} = -\bar{\alpha}\tan\bar{\alpha}$ and m odd to the pressure release condition giving $\bar{\nu} = \bar{\alpha}\cot\bar{\alpha}$. Approximate and exact (by this we mean that results were computed with sufficient accuracy) values of the roots $\bar{\alpha}_m$, $m = 0, 1, 2, \ldots$ are presented in Tables 1 and 2.

m	Approx.	Exact	$\bar{\nu} = -\bar{\alpha}\tan\bar{\alpha}$
0	2.3561 - 1.1216i	2.1061 - 1.1253i	1.6506 + 2.0599i
2	5.4977 - 1.5453i	5.3562 - 1.5515i	2.0578 + 5.3347i
4	8.6393 - 1.7713i	8.5366 - 1.7755i	2.2784 + 8.5226i
6	11.780 - 1.9263i	11.699 - 1.9294i	2.4311 + 11.688i

Table 1: First 4 double roots (EP2) for the hard wall condition (lower wall).

m	Approx.	Exact	$\bar{\nu} = \bar{\alpha}\cot\bar{\alpha}$
1	3.9269 - 1.3770i	3.7488 - 1.3843i	1.8952 + 3.7194i
3	7.0685 - 1.6709i	6.9499 - 1.6761i	2.1802 + 6.9329i
5	10.210 - 1.8548i	10.119 - 1.8583i	2.3605 + 10.107i
7	13.351 - 1.9889i	13.277 - 1.9915i	2.4929 + 13.268i

Table 2: First 4 double roots (EP2) for the pressure release condition (lower wall).

Only roots associated with absorbing boundary conditions (i.e. the imaginary part of $\bar{\nu}$ or equivalently the real part of the wall impedance must be positive) are shown. Other solutions associated with 'active' boundary conditions exist and are obtained from $\bar{\alpha}$ by taking the complex conjugate. To illustrate this in a more systematic way, it is convenient to study the values of the wall admittances on both sides in the complex-plane as a function of $\bar{\alpha} = (\mathrm{Re}\,\bar{\alpha}, \mathrm{Im}\,\bar{\alpha})$ as shown in Figure 1. This can be regarded as a representation of the EP2 complex $\bar{\alpha}$-plane since associated values of the wall parameters satisfy the double root condition and to each value of $\bar{\alpha}$ corresponds an unique pair of complex-valued wall-parameters $(\bar{\nu}, \bar{\mu})$ through Eqs (11). Three regions can be clearly identified: (i) a lower region with absorbing walls on both sides, (ii) an upper region with active walls on both sides and (iii) an intermediate region with both active and absorbing

walls. Particular roots corresponding to hard wall and pressure release conditions belong to a continuous curve that delimitates these regions. Dissipative scenarios of region (i) are usually discussed in the scientific literature as they can lead to practical realisations. Note that a similar description can be found in Kelsten's MSc Thesis (see Fig. 3.3 p. 18 in [14]).

There is a further set of interesting solutions satisfying the triple root condition:

$$K = K' = K'' = 0. \tag{14}$$

Following the previous derivation given by Eqs (7)-(9), it is easy to see that this condition leads to the existence of another wavefunction:

$$\psi'' = \partial_s^2 \psi = (Y'' + 2\mathrm{i}xY' - x^2 Y)\mathrm{e}^{\mathrm{i}sx}. \tag{15}$$

The additional constraint leads to the following equation for $\bar{\bar{\alpha}}$ where the double overbar is used to indicate that this is an EP3:

$$4\cos\bar{\bar{\alpha}} - \frac{\sin\bar{\bar{\alpha}}}{\bar{\bar{\alpha}}^2}(2\bar{\bar{\alpha}} + \sin(2\bar{\bar{\alpha}})) = 0. \tag{16}$$

It should be noted that whilst $\bar{\alpha}$ is a continuum, $\bar{\bar{\alpha}}$ comprises a discrete set of values. Koch gives an approximation for these roots [4]:

$$2\bar{\bar{\alpha}}_m \approx (2m+3)\pi - \mathrm{i}[\ln 2 + 2\ln((2m+3)\pi)] \quad m = 0, 1, 2, \ldots \tag{17}$$

There exit also purely real solutions which are not mentioned in Koch's paper, probably because they do not correspond to absorbing walls. These roots admit the following approximation:

$$2\bar{\bar{\alpha}}_m \approx (2m+3)\pi - \frac{2}{(2m+3)\pi}, \quad m = 0, 1, 2, \ldots \tag{18}$$

Approximate and exact values of the triple roots are presented in Tables 3 and 4 and also in Fig. 1. Wavefunctions associated with with purely real EP3 possess the particular property that, above cut-off, they propagate without any gain or attenuation with an amplification rate which is linear or quadratic since $|\psi'| \sim |xY|$ and $|\psi''| \sim |x^2 Y|$ for large x. We note in passing that this situation corresponds to the existence of real eigenvalues for non-Hermitian operators and this is typical of $\mathcal{PT}$-symmetric systems which have attracted intensive research interest in recent years (although the discussion is outside the scope of the present paper, we can cite for instance [21]).

Before we end this section we should note that numerical solutions of the dispersion equation, Eq. (6), as well as double and triple roots solutions of Eqs (12) and (16) are

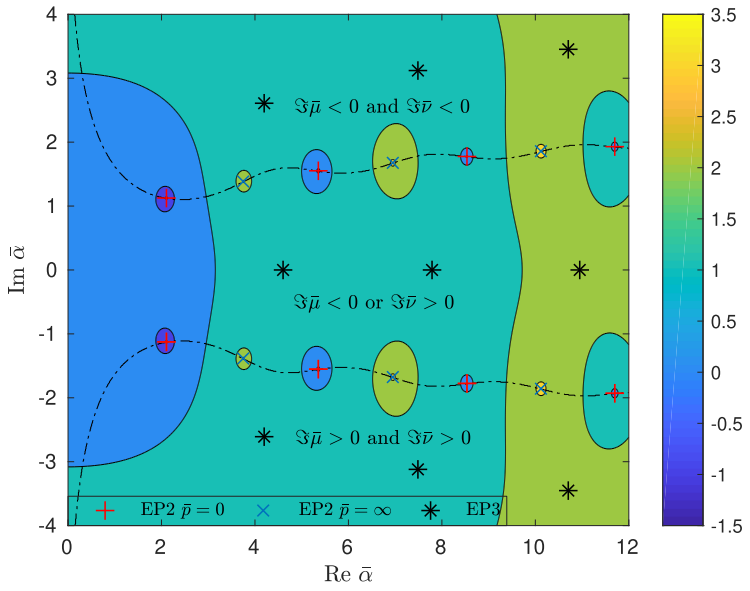

Figure 1: Representation of the EP2 complex $\bar{\alpha}$-plane. Isovalue of magnitude of the product of the two wall admittances in logarithmic scale ($\log_{10}|\bar{p}|$) is shown. Zeros and poles of $\bar{p}$ correspond to hard wall (see Tab. 1) and pressure release conditions (see Tab. 2) at one wall. The dash-dot lines correspond to $\mathrm{Im}\,\bar{\mu} = 0$ or $\mathrm{Im}\,\bar{\nu} = 0$. Star symbols correspond to EP3 points associated with the existence of wavefunctions satisfying the triple root condition (14) (see Tab. 3 and 4).

m	Approx.	Exact	$\bar{\bar{\nu}}$	$\bar{\bar{\mu}}$
0	4.7123 - 2.5899i	4.1969 - 2.6086i	3.1781+ 4.6751i	3.0875 + 3.6234i
1	7.8539 - 3.1007i	7.4869 - 3.1202i	3.6598 + 7.9684i	3.6015 + 6.9459i
2	10.995 - 3.4372i	10.7044 - 3.4525i	3.9800 + 11.189i	3.9371 + 10.176i
3	14.137 - 3.6885i	13.893 - 3.7006i	4.2215 + 14.380i	4.1876 + 13.372i
4	17.278 - 3.8891i	17.068 - 3.8989i	4.4158 + 17.556i	4.3877 + 16.550i

Table 3: First 5 triple roots (EP3) associated with absorbing conditions.

m	Approx.	Exact	$\bar{\bar{\nu}}(+), \bar{\bar{\mu}}(-)$
0	4.6062	4.6015	1.0119 ± 4.6029i
1	7.7903	7.7893	1.0041 ± 7.7896i
2	10.950	10.949	1.0020 ± 10.949i
3	14.101	14.101	1.0012 ± 14.101i
4	17.249	17.249	1.0008 ± 17.249i

Table 4: First 5 triple roots (EP3) associated with active and absorbing conditions on the real axis. Large order values can be estimated simply via $\bar{\bar{\nu}}_m \approx 1 + \mathrm{i}\bar{\bar{\alpha}}_m$.

computed with the method proposed in [22] and implemented for a dissipative silencer by the present authors in [23]. The approach which is based on Cauchy's theorem allows the zeros of analytic functions to be located within a closed path in the complex plane. The quality of the solution can be checked by substituting the roots into the dispersion equation and a refinement strategy is also possible around each root in order to increase the accuracy.

3. Perturbation analysis and optimality

In the dissipative scenario where both walls are absorbing, it is advocated in many papers, that double root solutions are optimal in the sense that coalescence of the first two modes coalesce yields optimal treatment in the sense that this should provide the best attenuation, i.e. the associated axial wave number has the strongest imaginary part. The reason for this can be found by looking at the behaviour of the solution in the vicinity of the optimal point. To do this, we introduce parameters $\delta = \nu - \bar{\nu}$ and $\epsilon = s - \bar{s}$ and try to identify the relationship between these two quantities. The starting point for the analysis is to consider a Taylor expansion of K around $(\bar{s}, \bar{\mu})$ while the admittance of the lower wall $\bar{\mu}$ is kept fixed. Thus,

$$K(s, \bar{\mu}, \nu) = \sum_{i=0}^{\infty} \sum_{j=0}^{\infty} \frac{\epsilon^i \delta^j}{i! j!} \partial_s^i \partial_\nu^j K(\bar{s}, \bar{\mu}, \bar{\nu}). \tag{19}$$

Note that, this series simplifies significantly since $\partial_s^i \partial_\nu^j K(\bar{s}, \bar{\mu}, \bar{\nu}) = 0$ for $j \geq 2$ and

$$Y(s, \mu, 1) = \partial_\nu K(s, \mu, \nu). \tag{20}$$

Further, we can make the analysis tractable by adopting the following notations:

$$K_i = \frac{\partial_s^i K(\bar{s}, \bar{\mu}, \bar{\nu})}{i!} \quad \text{and} \quad Y_i = \frac{\partial_s^i \partial_\nu K(\bar{s}, \bar{\mu}, \bar{\nu})}{i!} = \frac{\partial_s^i Y(\bar{s}, \bar{\mu}, 1)}{i!} \tag{21}$$

and this gives

$$\begin{aligned} K(s,\bar{\mu},\nu) &= K_0 + \epsilon K_1 + \epsilon^2 K_2 + \epsilon^3 K_3 + \epsilon^4 K_4 + \epsilon^5 K_5 + \ldots \\ &+ \delta(Y_0 + \epsilon Y_1 + \epsilon^2 Y_2 + \epsilon^3 Y_3 + \epsilon^4 Y_4 + \ldots) \end{aligned} \tag{22}$$

By construction $K(s,\bar{\mu},\nu)$ is zero everywhere. Thus, the double root condition, $K_0 = K_1 = 0$, leads to the equation

$$\epsilon^2 K_2 + \epsilon^3 K_3 + \epsilon^4 K_4 + \epsilon^5 K_5 + \delta(Y_0 + \epsilon Y_1 + \epsilon^2 Y_2 + \epsilon^3 Y_3 + \epsilon^4 Y_4) + \ldots = 0. \tag{23}$$

This Taylor series can be inverted, at least locally by assuming small perturbations, using a Puiseux series expansion. To do this, we shall assume for the moment that $K_2 \neq 0$ so that we can formally write

$$\epsilon = a\sqrt{\delta} + b\delta + \ldots \tag{24}$$

which, after substitution, gives the explicit form for the expansion coefficients

$$a^2 = -\frac{Y_0}{K_2} \quad \text{and} \quad b = Ba^2 \quad \text{with} \quad B = \frac{1}{2}\left(\frac{Y_1}{Y_0} - \frac{K_3}{K_2}\right). \tag{25}$$

Eqs (23) - (24) indicate that $\bar{\nu}$ is a branch point in the complex ν-plane so the variation in s is infinitely sensitive as $(\nu - \bar{\nu})$ tends to zero. That this should provide an optimal value, at least locally, can be understood from a graphical point of view as the two eigenvalues, call them s_1 and s_2, coalesce in opposite directions and in fact

$$\epsilon_n = s_n - \bar{s} = (-1)^n a\sqrt{\delta} + Ba^2\delta + \ldots, \quad n = 1, 2. \tag{26}$$

The result is a generalization of Tester's formula corresponding to the specific case of one rigid wall, i.e. $\bar{\mu} = 0$.

When the triple root condition is satisfied, $K_2 = 0$ and the Puiseux series Eq. (24) breaks down. To remedy this, one needs to seek an alternative expansion of the form

$$\epsilon = a\delta^{1/3} + b\delta^{2/3} + c\delta + \ldots \tag{27}$$

which, after substitution, gives the explicit form for the expansion coefficients

$$a^3 = -\frac{Y_0}{K_3}, \quad b = Ba^2 \quad \text{and} \quad c = Ca^3 \tag{28}$$

where

$$B = \frac{1}{3}\left(\frac{Y_1}{Y_0} - \frac{K_4}{K_3}\right) \tag{29}$$

$$C = \frac{1}{3}\left[\left(\frac{K_4}{K_3}\right)^2 + \frac{Y_2}{Y_0} - \frac{Y_1}{Y_0}\frac{K_4}{K_3} - \frac{K_5}{K_3}\right] \tag{30}$$

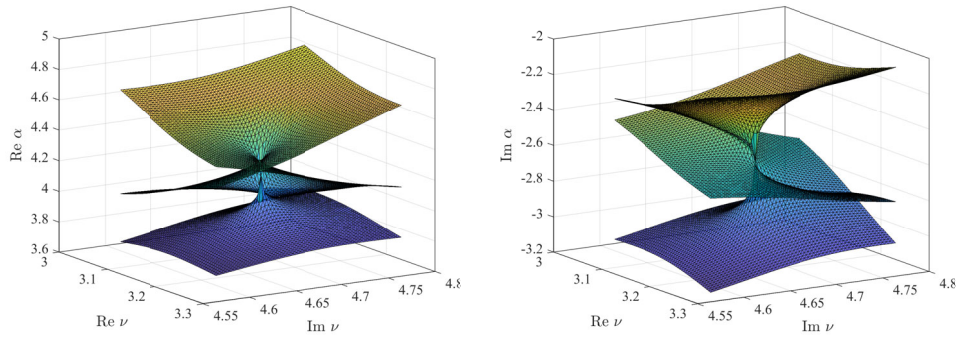

(a) (b)

Figure 2: Computed roots of the dispersion equation Eq. (6) showing the coalescence of 3 classical modes in the vicinity of an EP3. The real part of α is given in (a) and the imaginary part in (b).

In the close vicinity of the triple root, the three eigenvalues coalesce as follows

$$\epsilon_n = s_n - \bar{\bar{s}} = z^n a\,\delta^{1/3} + z^{2n} B a^2\,\delta^{2/3} + C a^3\,\delta + \ldots, \quad n = 1, 2, 3 \tag{31}$$

where $z^3 = 1$ is the cube root of unity. In order to illustrate this, it is convenient to consider the variation of the transverse wavenumber α. It is found that, to leading order

$$\alpha_n = \bar{\bar{\alpha}} + z^n\,\delta^{1/3}\left(-3!\,\frac{\partial_\nu K(\bar{\bar{s}}, \bar{\bar{\mu}}, \bar{\bar{\nu}})}{\partial_\alpha^3 K(\bar{\bar{s}}, \bar{\bar{\mu}}, \bar{\bar{\nu}})}\right)^{1/3} + \mathcal{O}(\delta^{2/3}), \quad n = 1, 2, 3. \tag{32}$$

Take the first triple root $\bar{\bar{\alpha}}_0 = 4.1969 - 2.6086\mathrm{i}$ given in Table 3 for instance, we find that

$$\alpha_n \approx \bar{\bar{\alpha}}_0 + z^n\,(\nu - \bar{\bar{\nu}}_0)^{1/3}(0.6886 - 0.7678\mathrm{i}), \tag{33}$$

with $\bar{\bar{\nu}}_0 = 3.1781 + 4.6751\mathrm{i}$. In Fig. 2, computed roots of the dispersion equation Eq. (6) showing the coalescence of 3 classical modes in the vicinity of the triple root $\bar{\bar{\alpha}}_0$ are shown. The real part of α, which gives the attenuation of waves at low frequency, reaches a maximum value at the EP3 which means that the latter corresponds to an optimal treatment. Another way to observe the crossing of modes is shown in Fig. 3 where trajectories of the roots in the complex plane are illustrated (left) by solving Eq. (6) (recall that $\nu = \delta + \bar{\bar{\nu}}_0$) by gradually varying δ on the real axis from -0.1 (indicated by the "+") to 0.1 (indicated by the "o"). The right hand figure shows the trajectories using the leading order expression Eq. (33) which gives a reasonable approximation. Values, represented as black squares, are calculated using the same incremental step for both figures and this shows how sensitive modal solutions are near EP3.

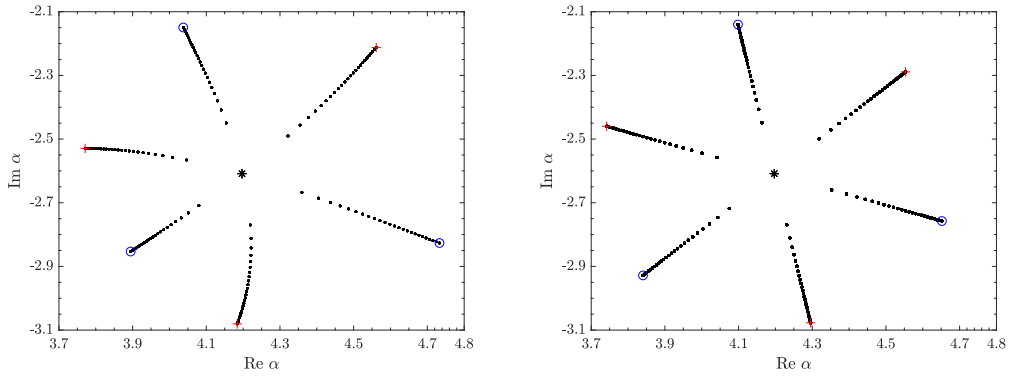

Figure 3: Trajectories of the roots on the complex plane in the vicinity of an EP3. Values are either computed from the dispersion equation (left) or given by the leading order approximation Eq. (33) (right).

The question now arises as to whether the exceptional points EP3 give best attenuation in all cases. To investigate this, we consider the following linear trajectory for the tranverse wavenumber in the EP2 $\bar{\alpha}$ complex plane as defined earlier:

$$\bar{\alpha} = \bar{\alpha}_0(1-\eta) + \bar{\bar{\alpha}}_0\eta, \quad \eta \geq 0, \tag{34}$$

where parameter η is a positive real number and $\bar{\alpha}_0$ corresponds to the first solution of the hard wall case ($\nu = 0$) (see Table 1). Thus, when $\eta = 0$ we are at the red star in Figure 5 a). As η is incrementally increased the corresponding values of the wall admittances $\bar{\mu}$ and $\bar{\nu}$, which must be regarded as functions of $\bar{\alpha}$, are calculated via Eq. (11); their trajectories are represented in Figure 4 and show a cusp at the triple root (EP3). For each pair $(\bar{\mu}, \bar{\nu})$, the first four roots of the dispersion relation

$$(\bar{\nu} + \bar{\mu})\cos\alpha + \left(\alpha - \frac{\bar{\nu}\bar{\mu}}{\alpha}\right)\sin\alpha = 0, \tag{35}$$

(where it is understood that $\bar{\nu} = \nu(\bar{\alpha})$ and $\bar{\mu} = \mu(\bar{\alpha})$) are calculated and their trajectories are plotted in Figure 5 (a).

One recognizes the linear path given by Eq. (34) and other trajectories correspond to classical modes (i.e. single roots). The coalescence of one of these modes with the double root occurs at $\bar{\bar{\alpha}}_0$ as expected. Note the coalescence is somehow atypical as is does not correspond to the merging of three classical modes and the description made earlier in Eq. (32) does not hold in this case. Corresponding axial wavenumbers are shown in Figures 5 (b)(c) and (d) for three frequencies $k = \pi/10$, π and 3π. At low frequency, $\bar{s} \approx \mathrm{i}\bar{\alpha}$ which corresponds to a rotation of $\pi/2$ as shown in Figure 5 (b) and the gain, in terms

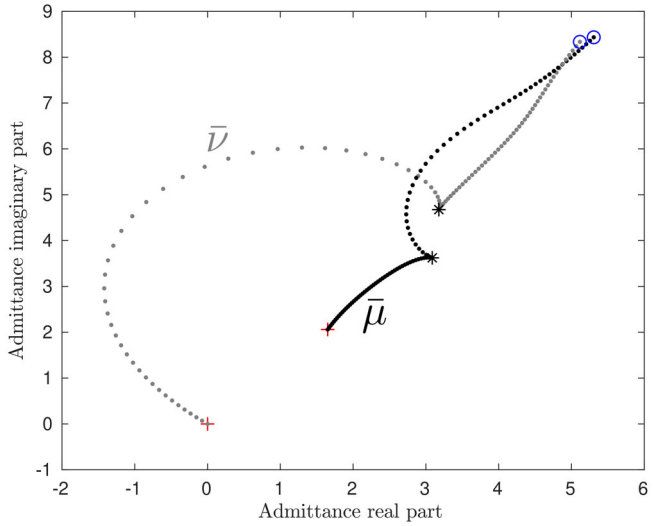

Figure 4: Trajectories of the wall admittances associated with Eq. (34). The red stars indicate the $\eta = 0$ points and the black stars indicate the EP3 as given in first line of Tab. 3.

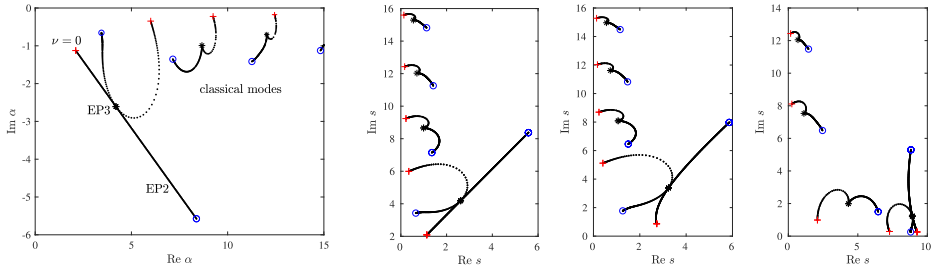

(a) (b) $k = \pi/10$ (c) $k = \pi$ (d) $k = 3\pi$

Figure 5: Trajectories of the first transverse (a) and first axial wavenumbers for three frequencies (b)-(d).

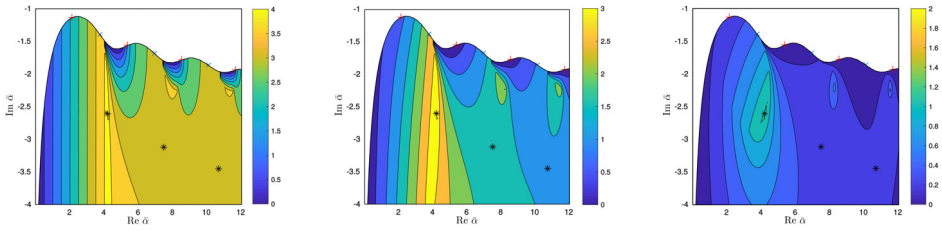

(a) $k = 0.1\pi$ (b) $k = \pi$ (c) $k = 3\pi$

Figure 6: Attenuation of the least attenuated mode showing that the triple root $\bar{\bar{\alpha}}_0 = 4.1969 - 2.6086\mathrm{i}$ provides the optimum condition. The colorbar indicates the imaginary of the axial wavenumber.

of attenuation, is quite substantial when compared to the first Tester's optimal value $\bar{\alpha}_0$ for the hard wall case, i.e. the imaginary part of the axial wavenumber is nearly twice as large at EP3. At higher frequency, the attenuation decreases but in every case considered, EP3 leads to best attenuation. In order to see this in more systematic way, let us consider again the EP2 $\bar{\alpha}$ complex plane (we shall limit the analysis to the dissipative region (i) here). For each value of $\bar{\alpha}$, discrete solutions of Eq. (35) are computed and the imaginary part of the axial wavenumber s corresponding to the least attenuated mode is reported in Fig. 6. Results clearly suggest that the EP3 for the first triple root $\bar{\bar{\alpha}}_0$ provide the optimal pair of admittances $(\bar{\bar{\nu}}_0, \bar{\bar{\mu}}_0)$ given in Table 3. As already discussed earlier (and also in Tester's original paper [1] for the hard wall case $\mu = 0$), this optimum condition is offset by an amplification rate which varies linearly and/or quadratically with distance and in fact $|\psi'| \sim |x\psi|$ and $|\psi''| \sim |x^2\psi|$ where $|\psi| = |Y| \exp\left[-x \operatorname{Im}(k^2 - \bar{\bar{\alpha}}_0^2)^{1/2}\right]$. To the authors' knowledge this result has never been presented in the scientific literature. The attenuation rate of the mean square modal amplitude (the amplification being now ignored) is proportional to the imaginary part of the axial wavenumber, and in the usual units the attenuation is $8.69 \operatorname{Im} s$ dB per duct width. For the sake of illustration, numerical values are reported in Fig. 7 for three cases of special interest (note $k = \pi$ corresponds to the first cut-off frequency in a duct with rigid walls).

4. Green's function

4.1. Classical case

It is well known that the Green's function, which satisfies

$$(\partial_{xx}^2 + \partial_{yy}^2 + k^2) G(\boldsymbol{x}, \boldsymbol{x}_0) = \delta(x - x_0)\delta(y - y_0) \tag{36}$$

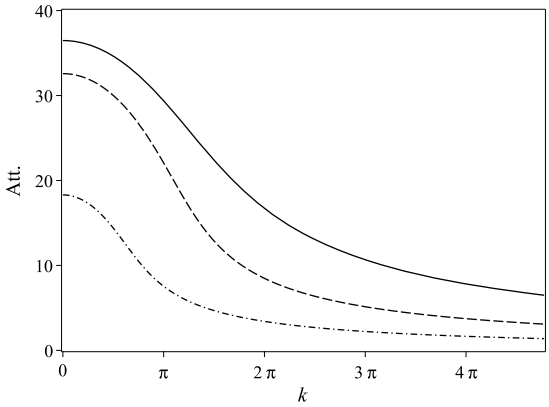

Figure 7: Comparison of attenuation rate (in dB per duct width) for three scenarios: (i) optimal condition (with $\bar{\bar{\alpha}}_0$, see Table 3) (solid line); (ii) optimal condition with one rigid wall (with $\bar{\alpha}_0$, see Table 1) (dash-dot); (iii) optimal condition with pressure release condition (dashed) at one wall (with $\bar{\alpha}_1$, see Table 2).

where $\boldsymbol{x} = (x, y)$ and $\boldsymbol{x}_0 = (x_0, y_0)$ are the evaluation and the source point, can be constructed elegantly using a Fourier-transform and subsequent application of the residue theorem in the complex plane [26]. Simple poles are associated with classical duct modes and the occurrence of a higher order pole signifies that these modes are of a different nature. The procedure used in the present work, however, follows Tester's derivation [1]. The starting point is to express the Green's function as an infinite series of the form

$$G(\boldsymbol{x}, \boldsymbol{x}_0) = \sum_{n=1}^{\infty} \frac{\Psi(s_n, \boldsymbol{x}, \boldsymbol{x}_0)}{2\mathrm{i} P_n s_n} \tag{37}$$

where

$$\Psi(s, \boldsymbol{x}, \boldsymbol{x}_0) = Y(s, \mu, y) Y(s, \mu, y_0) \mathrm{e}^{\mathrm{i}s|x - x_0|} \tag{38}$$

with the requirement that $\operatorname{Im} s \geq 0$ in the dissipative case. In Eq. (37), the α_n's are the discrete roots of the dispersion equation (6) and the ordering in the summation is by increasing imaginary part of axial wavenumber, s_n. Thus, s_1 is the least attenuated mode. The associated eigenfunctions, i.e. the duct acoustic mode are given explicitly by Eq. (3). The quantity P_n is calculated from the integral

$$P_n = \int_0^1 Y^2(s_n, \mu, y)\, \mathrm{d}y. \tag{39}$$

Note that following Lawrie's work [24, 25], it can be shown[1] that

$$P_n = -\frac{Y(s_n,\mu,1)}{2s_n}K'(s_n,\mu,\nu), \tag{40}$$

where the reader is reminded that the prime indications differentiation with respect to s. This result represents one of the main ingredients of the procedure as it establishes the deep connection between P_n and the dispersion equation of the waveguide eigenvalue problem. Thus, the series, which can take the alternate form

$$G(\boldsymbol{x},\boldsymbol{x}_0) = \sum_{n=1}^{\infty} \frac{\mathrm{i}\Psi(s_n,\boldsymbol{x},\boldsymbol{x}_0)}{Y(s_n,\mu,1)\,K'(s_n,\mu,\nu)}, \tag{41}$$

is only valid if $K' \neq 0$ for all modes involved in the series. The fact that P_n can be zero whenever we are facing the existence of an exceptional point, stems from the fact that Eq. (39) does not define a norm and in this case EP modes are said to be self-orthogonal.

4.2. Case of an EP2

In this scenario, the wall parameters $(\bar{\mu},\bar{\nu})$ correspond to the existence of an EP2 which means that one of the integrals in Eq. (39) is zero. To make progress, we must identify the pair of classical modes which lie close to the exceptional point. Without loss of generality, we might label these two modes with indices $n = 1$ and $n = 2$ and consider a slight deviation of the optimal admittance $\nu = \bar{\nu} + \delta$ while $\bar{\mu}$ is fixed. In the spirit of the previous section, we can use the regularity of function K' and expand it as a Taylor series around $\bar{s}$ and $\bar{\nu}$ (recall that $\epsilon = s - \bar{s}$):

$$\begin{aligned} K'(s,\bar{\mu},\nu) &= 2\epsilon K_2 + 3\epsilon^2 K_3 + 4\epsilon^3 K_4 + 5\epsilon^4 K_5 + \ldots \\ &+ \delta(Y_1 + 2\epsilon Y_2 + 3\epsilon^2 Y_3 + 4\epsilon^3 Y_4 + \ldots), \end{aligned} \tag{42}$$

and similarly with $\mu = \bar{\mu}$

$$Y(s,\bar{\mu},1) = Y_0 + \epsilon Y_1 + \epsilon^2 Y_2 + \epsilon^3 Y_3 + \epsilon^4 Y_4 + \ldots \tag{43}$$

For the moment we may assume that $K_2 \neq 0$ so we can use the Puiseux series expansion Eq. (26). Application of Taylor's expansion with respect to $(\bar{\mu},\bar{\nu})$, yields the asymptotic form

$$Y(s_n,\bar{\mu},1)\,K'(s_n,\bar{\mu},\nu) = (-1)^n \Lambda_1 \sqrt{\delta} + \Lambda_2 \delta + \ldots \tag{44}$$

[1] The specific case corresponding to the pressure release condition $Y(s_n,\mu,1) = 0$ is not included in the present analysis.

where

$$\Lambda_1 = 2aY_0K_2 \quad \text{and} \quad \frac{\Lambda_2}{\Lambda_1} = a\left(\frac{Y_1}{Y_0} + \frac{K_3}{K_2}\right). \tag{45}$$

Function Ψ can also be regarded as regular function with respect to s and it can be expanded around $\bar{s}$ as

$$\begin{aligned} \Psi(s_n, \boldsymbol{x}, \boldsymbol{x}_0) &= \Psi(\bar{s}, \boldsymbol{x}, \boldsymbol{x}_0) + \epsilon_n \Psi'(\bar{s}, \boldsymbol{x}, \boldsymbol{x}_0) + \dots \\ &= \Psi(\bar{s}, \boldsymbol{x}, \boldsymbol{x}_0)\left[1 + (-1)^n \Phi_1\, a\sqrt{\delta} + \dots\right] \end{aligned} \tag{46}$$

where, to ease the notation we put $\Psi'(\bar{s}, \boldsymbol{x}, \boldsymbol{x}_0) = \Phi_1\, \Psi(\bar{s}, \boldsymbol{x}, \boldsymbol{x}_0)$ with

$$\Phi_1 = \frac{Y'(\bar{s}, \bar{\mu}, y)}{Y(\bar{s}, \bar{\mu}, y)} + \frac{Y'(\bar{s}, \bar{\mu}, y_0)}{Y(\bar{s}, \bar{\mu}, y_0)} + \mathrm{i}|x - x_0|. \tag{47}$$

We can now calculate the limit for the first two terms of the series as follows

$$\begin{aligned} G^{\#}_{\mathrm{EP2}}(\boldsymbol{x}, \boldsymbol{x}_0) &= \lim_{\delta \to 0} \sum_{n=1,2} \frac{\mathrm{i}\Psi(s_n, \boldsymbol{x}, \boldsymbol{x}_0)}{Y(s_n, \bar{\mu}, 1)\, \partial_s K(s_n, \bar{\mu}, \nu)} \\ &= \mathrm{i}\Psi(\bar{s}, \boldsymbol{x}, \boldsymbol{x}_0) \lim_{\delta \to 0} \sum_{n=1,2} \frac{1 + (-1)^n \Phi_1\, a\sqrt{\delta} + \dots}{(-1)^n \Lambda_1 \sqrt{\delta} + \Lambda_2 \delta + \dots} \end{aligned} \tag{48}$$

After some manipulation, this can be given in the more compact and tractable form:

$$G^{\#}_{\mathrm{EP2}}(\boldsymbol{x}, \boldsymbol{x}_0) = \frac{\mathrm{i}\Psi(\bar{s}, \boldsymbol{x}, \boldsymbol{x}_0)}{Y_0 K_2}\left(\Phi_1 - \frac{Y_1}{Y_0} - \frac{K_3}{K_2}\right). \tag{49}$$

Thus, the Green's function for this case can be expressed as

$$G_{\mathrm{EP2}}(\boldsymbol{x}, \boldsymbol{x}_0) = \sum_{n=3}^{\infty} \frac{\Psi(s_n, \boldsymbol{x}, \boldsymbol{x}_0)}{2\mathrm{i}P_n s_n} + G^{\#}_{\mathrm{EP2}}(\boldsymbol{x}, \boldsymbol{x}_0). \tag{50}$$

As far as the authors' are aware, formula Eq. (50), which is one of the main results of this paper, does not appear in the scientific literature except for the hard wall scenario ($\bar{\mu} = 0$), investigated by Tester. Tester's result can be retrieved from Eqs (49)-(50), on noting that that $Y_0 = \cos\bar{\alpha}$ and $Y_1 = -\bar{\gamma}\sin\bar{\alpha}$ (here we defined $\bar{\gamma} = -\bar{s}/\bar{\alpha}$). Further, it can be shown that (see details in Appendix):

$$K_2 = \bar{\gamma}^2 \cos\bar{\alpha} \quad \text{and} \quad \frac{K_3}{K_2} = \frac{1 + \bar{\gamma}^2}{\bar{s}} - \frac{\bar{\gamma}}{3}\tan\bar{\alpha}. \tag{51}$$

So, from the characteristic equation associated with the hard wall condition, see Eq. (12), we obtain the following equalities:

$$\frac{\bar{\alpha}^2}{(\cos\bar{\alpha})^2} = -\bar{\alpha}\bar{t} \quad \text{and} \quad \bar{t}^2 + \frac{\bar{t}}{\bar{\alpha}} + 1 = 0 \quad \text{with} \quad \bar{t} = \tan\bar{\alpha}. \tag{52}$$

Thus, we can calculate

$$\frac{\mathrm{i}}{Y_0 K_2}\left(-\frac{Y_1}{Y_0} - \frac{K_3}{K_2}\right) = \mathrm{i}\frac{\bar{\alpha}}{\bar{s}^2}\,\bar{t}\left(\frac{1 + \bar{\gamma}^2}{\bar{s}} - \frac{4\bar{\gamma}}{3}\bar{t}\right) = \frac{\mathrm{i}}{\bar{s}^3}\left(\frac{\bar{s}^2}{3}\bar{t}^2 + \bar{\alpha}\bar{t} - \bar{s}^2\right). \tag{53}$$

Now, from Eq. (8) (with $\mu = 0$), we have $Y = \cos(\bar{\alpha}y)$ and $Y' = -\bar{\gamma}y\sin(\bar{\alpha}y)$. Thus,

$$\Phi_1 = -\bar{\gamma}y\tan(\bar{\alpha}y) - \bar{\gamma}y_0\tan(\bar{\alpha}y_0) + \mathrm{i}|x - x_0|, \tag{54}$$

and we find

$$\begin{aligned} G^{\#}_{\mathrm{EP2}}(\boldsymbol{x},\boldsymbol{x}_0) &= \cos(\bar{\alpha}y)\cos(\bar{\alpha}y_0)\mathrm{e}^{\mathrm{i}\bar{s}|x-x_0|} \\ &\times \left\{\frac{\bar{t}}{\mathrm{i}\bar{s}^2}\left(\bar{s}y_0\tan(\bar{\alpha}y_0) + \bar{s}y\tan(\bar{\alpha}y) + \mathrm{i}\bar{\alpha}|x-x_0|\right) + \frac{\mathrm{i}}{\bar{s}^3}\left(\frac{\bar{s}^2}{3}\bar{t}^2 + \bar{\alpha}\bar{t} - \bar{s}^2\right)\right\}, \end{aligned} \tag{55}$$

which is the exact form as reported (see Eq. (28) in [1]) [2].

4.3. Case of an EP3

In this scenario, $K_2 = 0$ and expression Eq. (49) is no longer valid. We need to use the fact that three eigenvalues, labelled $n = 1, 2, 3$, coalesce at EP3 associated with the pair of wall parameters $(\bar{\bar{\nu}}, \bar{\bar{\mu}})$ and their trajectories are described by the Puiseux series Eq. (31) with $\delta = \mu - \bar{\bar{\mu}}$. Following the previous derivation, we find

$$Y(s_n, \bar{\bar{\mu}}, 1)\, K'(s_n, \bar{\bar{\mu}}, \nu) = z^{2n}\,\Lambda_1\,\delta^{2/3} + \Lambda_2\,\delta + z^{4n}\,\Lambda_3\,\delta^{4/3} + \ldots, \tag{56}$$

where

$$\Lambda_1 = 3a^2 Y_0 K_3, \quad \frac{\Lambda_2}{\Lambda_1} = -\frac{2a}{3}\left(2\frac{Y_1}{Y_0} + \frac{K_4}{K_3}\right), \tag{57}$$

and

$$\frac{\Lambda_3}{\Lambda_1} = \frac{a^2}{9}\left[7\left(\frac{Y_1}{Y_0}\right)^2 + 7\frac{Y_1}{Y_0}\frac{K_4}{K_3} - 5\left(\frac{K_4}{K_3}\right)^2 + 3\left(\frac{Y_2}{Y_0} + \frac{K_5}{K_3}\right)\right]. \tag{58}$$

Again, we shall use the fact that function Ψ is a regular function of s and we can expand it around $\bar{\bar{s}}$ as (we need to expand the function up to second order here):

$$\Psi(s_n, \boldsymbol{x}, \boldsymbol{x}_0) = \Psi(\bar{\bar{s}}, \boldsymbol{x}, \boldsymbol{x}_0) + \epsilon_n\Psi'(\bar{\bar{s}}, \boldsymbol{x}, \boldsymbol{x}_0) + \frac{1}{2}\epsilon_n^2\Psi''(\bar{\bar{s}}, \boldsymbol{x}, \boldsymbol{x}_0) + \ldots. \tag{59}$$

To ease the notation, we introduce function Φ_2 defined such that $\Psi'' = \Phi_2\Psi$ and

$$\begin{aligned} \Phi_2 &= \frac{Y''(\bar{\bar{s}}, \bar{\bar{\mu}}, y)}{Y(\bar{\bar{s}}, \bar{\bar{\mu}}, y)} + \frac{Y''(\bar{\bar{s}}, \bar{\bar{\mu}}, y_0)}{Y(\bar{\bar{s}}, \bar{\bar{\mu}}, y_0)} - (x - x_0)^2 \\ &+ 2\frac{Y'(\bar{\bar{s}}, \bar{\bar{\mu}}, y)}{Y(\bar{\bar{s}}, \bar{\bar{\mu}}, y)}\frac{Y'(\bar{\bar{s}}, \bar{\bar{\mu}}, y_0)}{Y(\bar{\bar{s}}, \bar{\bar{\mu}}, y_0)} + 2\mathrm{i}|x - x_0|\left(\frac{Y'(\bar{\bar{s}}, \bar{\bar{\mu}}, y)}{Y(\bar{\bar{s}}, \bar{\bar{\mu}}, y)} + \frac{Y'(\bar{\bar{s}}, \bar{\bar{\mu}}, y_0)}{Y(\bar{\bar{s}}, \bar{\bar{\mu}}, y_0)}\right). \end{aligned} \tag{60}$$

We finally find the following expansion of Puiseux type

$$\Psi(s_n, \boldsymbol{x}, \boldsymbol{x}_0) = \Psi(\bar{\bar{s}}, \boldsymbol{x}, \boldsymbol{x}_0)\left[1 + z^n\Phi_1\, a\delta^{1/3} + z^{2n}\left(B\Phi_1 + \frac{\Phi_2}{2}\right)a^2\delta^{2/3} + \ldots\right], \tag{61}$$

[2] In Tester's paper, the width of the waveguide is h and Eq. (28) is recovered by simply replacing transverse and axial wavenumbers $\bar{\alpha}$ and $\bar{s}$ by $k_{yn}\,h$ and $k_{xn}\,h$. Note that the two formulae differ by a factor 2 which is due to the form of the Green's function series given in Eq. (20) in [1].

where coefficient B is given explicitly in Eq. (29) and function Φ_1 is defined in Eq. (47) (with $\bar{s}$, $\bar{\mu}$ replaced by $\bar{\bar{s}}$, $\bar{\bar{\mu}}$). We can now calculate the limit

$$\begin{aligned} G^{\#}_{\mathrm{EP3}}(\boldsymbol{x},\boldsymbol{x}_0) &= \mathrm{i}\Psi(\bar{\bar{s}},\boldsymbol{x},\boldsymbol{x}_0)\lim_{\delta\to 0}\sum_{n=1}^{3}\frac{1+z^n\Phi_1\,a\delta^{1/3}+z^{2n}\left[B\Phi_1+\frac{\Phi_2}{2}\right]a^2\delta^{2/3}+\ldots}{z^{2n}\,\Lambda_1\,\delta^{2/3}+\Lambda_2\,\delta+z^{4n}\,\Lambda_3\,\delta^{4/3}+\ldots} \\ &= \frac{\mathrm{i}\Psi(\bar{\bar{s}},\boldsymbol{x},\boldsymbol{x}_0)}{\Lambda_1}\lim_{\delta\to 0}\left[\delta^{-2/3}\sum_{n=1}^{3}z^{-2n}+\delta^{-1/3}\sum_{n=1}^{3}\left(\Phi_1 a z^{-n}-\frac{\Lambda_2}{\Lambda_1}z^{-4n}\right)\right. \\ &\quad \left.+\sum_{n=1}^{3}\left((B\Phi_1+\frac{\Phi_2}{2})a^2-\frac{\Lambda_3}{\Lambda_1}+\frac{\Lambda_2^2}{\Lambda_1^2}z^{-6n}-\Phi_1 a\frac{\Lambda_2}{\Lambda_1}z^{-3n}\right)\right]. \end{aligned} \tag{62}$$

After using the cubic root identity (j and p are arbitrary integers):

$$\sum_{n=1}^{3}z^{jn}=3\delta_{j,3p}, \tag{63}$$

(where $z^3=1$ and $\delta_{j,m}$ is the usual Kronecker delta function), the singular terms disappear and this finally leads to

$$G^{\#}_{\mathrm{EP3}}(\boldsymbol{x},\boldsymbol{x}_0)=\frac{3\mathrm{i}\Psi(\bar{\bar{s}},\boldsymbol{x},\boldsymbol{x}_0)}{\Lambda_1}\left[\frac{\Lambda_2^2}{\Lambda_1^2}-\frac{\Lambda_3}{\Lambda_1}-\Phi_1 a\frac{\Lambda_2}{\Lambda_1}+\left(B\Phi_1+\frac{\Phi_2}{2}\right)a^2\right]. \tag{64}$$

This can be recast in the final form

$$G^{\#}_{\mathrm{EP3}}(\boldsymbol{x},\boldsymbol{x}_0)=\frac{\mathrm{i}\Psi(\bar{\bar{s}},\boldsymbol{x},\boldsymbol{x}_0)}{Y_0K_3}\left[\Lambda-\Phi_1\left(\frac{Y_1}{Y_0}+\frac{K_4}{K_3}\right)+\frac{\Phi_2}{2}\right], \tag{65}$$

where

$$\Lambda=\left(\frac{Y_1}{Y_0}+\frac{K_4}{K_3}\right)^2-\frac{Y_1}{Y_0}\frac{K_4}{K_3}+\frac{Y_2}{Y_0}+\frac{K_5}{K_3} \tag{66}$$

which has a similar structure to Eq. (49). Closed forms expressions for all variables involved Y_i and K_i can be found in the Appendix. Finally, the Green's function for the EP3 scenario can be expressed as

$$G_{\mathrm{EP3}}(\boldsymbol{x},\boldsymbol{x}_0)=\sum_{n=4}^{\infty}\frac{\Psi(s_n,\boldsymbol{x},\boldsymbol{x}_0)}{2\mathrm{i}P_n s_n}+G^{\#}_{\mathrm{EP3}}(\boldsymbol{x},\boldsymbol{x}_0). \tag{67}$$

5. Conclusions

A comprehensive analysis of the first two exceptional points (EP2 and EP3) has been presented for a two-dimensional waveguide with arbitrary admittance boundary conditions on both sides of the guide. It has been confirmed that $\bar{\alpha}$ (the double root corresponding to EP2) is a continuum, that is to each value of $\bar{\alpha}$ there corresponds a unique pair of complex-valued wall parameters $(\bar{\nu},\bar{\mu})$, whilst $\bar{\bar{\alpha}}$ admits only discrete values. An EP is formed by the coalescence of two (or three) nearby eigenvalues (axial wavenumbers)

and this process has been studied using a perturbation method. The dispersion relation was expressed as a double Taylor series which was then inverted using a Puiseux expansion to obtain approximate expressions for the coalescing eigenvalues in terms of $\bar{s}$ and $\bar{\bar{s}}$ for fixed $\bar{\mu}$ as $\nu \to \bar{\nu}$ (see Eqs (26) and (31)). The trajectories predicted by Eq. (31) have been compared with those obtained by numerical solution of the dispersion relation and good agreement has be shown (Figure 3). Further, Figures 5 and 6 suggest that optimum attenuation is achieved at EP3, although there is scope for further analytic/numerical work to verify this.

The Green's function for the eigensystem has been considered. It has been demonstrated that the classical expression for the Green's function is degenerate at an EP. An analogous process to that used to study the coalescence of the eigenvalues, has enabled the authors to present modified Green's functions which are valid at EP2 and EP3. These contain additional terms which ensure the completeness of the eigenfunctions in these cases. It is worth commenting that standard mode-matching methods do not satisfactorily address the cases of EP2 and EP3 (such methods are, however, valid close to EP and have been used to investigate problems in this context). It is anticipated that the additional terms seen in the Greens functions must be incorporated into, and thus modify, the mode-matching procedure at EP. This is a topic of current investigation by the authors.

To conclude, the methods and results presented in this paper pave the way for complementary studies, for example, of the eigensystem underpinning the boundary value problem studied herein and/or of exceptional points in waveguides with wavebearing boundaries. It is anticipated that the results will be of use in various applications where noise control is desirable.

References

[1] B.J. Tester, The optimisation of modal sound attenuation in ducts, in the absence of mean flow, J. Sound Vib. (1973), 27, 477–513.

[2] L. Cremer, Theory regarding the attenuation of sound transmitted by air in a rectangular duct with an absorbing wall, and the maximum attenuation constant produced during this process, Acustica (1953), 3, 249–263.

[3] W.E. Zorumski, J.P. Mason, Multiple eigenvalues of sound-absorbing circular and annular ducts, J. Acoust. Soc. Am. (1974), 55, 1158–1165.

[4] W. Koch, Attenuation of sound in multi-element acoustically lined rectangular ducts in the absence of mean flow, J. Sound Vib. (1977), 52, 459–496.

[5] R. Kabral, L. Du, M. Åbom, Optimum sound attenuation in flow ducts based on the "exact" Cremer impedance. Acta Acustica united with Acustica (2016), 102, 851–860.

[6] X. Qiu, L. Du, X. Jing, X. Sun. The Cremer concept for annular ducts for optimum sound attenuation. J. Sound Vib. (2019), 438, 383–401.

[7] Z. Zhang, H. Boden, M. Åbom. The Cremer impedance: An investigation of the low frequency behavior. J. Sound Vib. (2019), 459, 114844.

[8] L. Xiong, B. Nennig, Y. Aurégan, W. Bi, Sound attenuation optimization using metaporous materials tuned on exceptional points, J. Acoust. Soc. Am. (2017), 142, 2288–2297.

[9] A. Spillere, J. Cordioli, Optimum acoustic impedance in circular ducts with inviscid sheared flow: Application to turbofan engine intake, J. Sound Vib. (2019), 443, 502–519.

[10] J.R. Sánchez, E. Piot, G. Casalis, Theoretical and numerical investigation of optimal impedance in lined ducts with flow, Acoustics 2012, Nantes, France.

[11] E.L. Shenderov. Helmholtz equation solutions corresponding to multiple roots of the dispersion equation for a waveguide with impedance walls, Acoust. Phys. (2000), 46(3), 357–363.

[12] W. Bi, V. Pagneux, New insights into mode behaviours in waveguides with impedance boundary conditions, arXiv:1511.05508. (2015).

[13] W. Guo, J. Liu, W. Bi, D. Yang, Y. Aurégan, V. Pagneux. Spatial transient behavior in waveguides with lossy impedance boundary conditions. arXiv preprint arXiv:2010.03646, (2020).

[14] M. Kelsten, Modeling of acoustic waves in pipes with impedance walls and double roots, Rutgers University-School of Graduate Studies, Oct. 2018.

[15] B. Nennig and E. Perrey-Debain, A high order continuation method to locate exceptional points and to compute puiseux series with applications to acoustic waveguides. J. Comp. Phys. (2020), 109425.

[16] P.M. Morse, K.U. Ingard, Theoretical acoustics, (McGraw-Hill Book Company, New York, 1968), Chap. IX.

[17] B. Midya, V. Konotop, Modes and exceptional points in waveguides with impedance boundary conditions, Optics Letters (2016), 20, 4621–4624.

[18] J. Doppler *et al.*, Dynamically encircling exceptional points in a waveguide: asymmetric mode switching from the breakdown of adiabaticity, Nature (2016), 537, 76–79.

[19] K. Ding, G. Ma, M. Xiao, Z.Q. Zhang, C.T. Chan, Emergence, coalescence, and topological properties of multiple exceptional points and their experimental realization, Physical Review X (2016) 6, 021007.

[20] W.D. Heiss, Greens functions at exceptional points, International Journal of Theoretical Physics (2015) 54, 3954–3959.

[21] J. Schnabel, H. Cartarius, J. Main, G. Wunner, W.D. Heiss, PT-symmetric wave guide system with evidence of a third-order exceptional point, Phys. Rev. A (2017) 95, 053868.

[22] L.M. Delves, J.N. Lyness. A numerical method for locating the zeros of an analytic function, Math. Comp. (1967), 21, 543–560.

[23] B. Nennig, E. Perrey-Debain, M. Ben Tahar. A mode matching method for modelling dissipative silencers lined with porous elastic materials and containing mean flow, J. Acoust. Soc. Am. (2010), 128(6), 3308–3320.

[24] J. B. Lawrie, On eigenfunction expansions associated with wave propagation along ducts with wave-bearing boundaries, IMA Journal of Applied Mathematics (2007), 72(3), 376-394.

[25] J. B. Lawrie, On acoustic propagation in three-dimensional rectangular ducts with flexible walls and porous linings, J. Acoust. Soc. Am. (2012), 131(3), 1890–1901.

[26] S.W. Rienstra, B.J. Tester, An analytic Green's function for a lined circular duct containing uniform mean flow, J. Sound Vib. (2008), 317 (3-5), 994–1016.

Appendix A. Derivatives of the dispersion equation

We recall that ($p = \nu\mu$ and $q = \nu + \mu$)

$$K = q\,\cos\alpha + \alpha\sin\alpha - g(\alpha)p, \tag{A.1}$$

where $g = \sin(\alpha)/\alpha$ stands for the cardinal sine function. Following standard algebra, we obtain

$$\partial_\alpha K = (1-\nu-\mu)\sin\alpha + \alpha\cos\alpha - g'(\alpha)p, \tag{A.2}$$

and

$$\partial_\alpha^2 K = -K + 2\cos\alpha + 2h(\alpha)p, \tag{A.3}$$

with $h(\alpha) = g'(\alpha)/\alpha$, here symbol $'$ means differentiation with respect to α and this notation is only adopted in this Appendix. Finally, straightforward calculations yield

$$\partial_\alpha^3 K = -\partial_\alpha K\ - 2\sin\alpha + 2h'(\alpha)p, \tag{A.4}$$

$$\partial_\alpha^4 K = -\partial_\alpha^2 K - 2\cos\alpha + 2h''(\alpha)p, \tag{A.5}$$

$$\partial_\alpha^5 K = -\partial_\alpha^3 K + 2\sin\alpha + 2h'''(\alpha)p. \tag{A.6}$$

Function K can also be regarded as a regular function of the axial wavenumber s. By applying the chain rule: $\partial_s \equiv \gamma\,\partial_\alpha$ where $\gamma = -s/\alpha$ repeatedly, we can calculate

$$K_2 = \bar\gamma^2[h(\bar\alpha)\,\bar p + \cos\bar\alpha] \tag{A.7}$$

$$\frac{K_3}{K_2} = \frac{1+\bar\gamma^2}{\bar s} + \frac{\bar\gamma}{3}\frac{h'(\bar\alpha)\,\bar p - \sin\bar\alpha}{h(\bar\alpha)\,\bar p + \cos\bar\alpha} \tag{A.8}$$

where it is reminded that the overbar symbol relates to EP2.

In the scenario of EP3 (identified with double overbar symbols), the calculations are somewhat tedious but it can be shown that:

$$K_3 = \frac{\bar{\bar\gamma}^3}{3}[h'(\bar{\bar\alpha})\,\bar{\bar p} - \sin\bar{\bar\alpha}], \tag{A.9}$$

$$\frac{K_4}{K_3} = \frac{\bar{\bar\gamma}}{4}\frac{h''(\bar{\bar\alpha})\,\bar{\bar p} - \cos\bar{\bar\alpha}}{h'(\bar{\bar\alpha})\,\bar{\bar p} - \sin\bar{\bar\alpha}} + \frac{3(1+\bar{\bar\gamma}^2)}{2\bar{\bar s}}, \tag{A.10}$$

$$\frac{K_5}{K_3} = \frac{\bar{\bar\gamma}^2}{20}\frac{h'''(\bar{\bar\alpha})\,\bar{\bar p} + \sin\bar{\bar\alpha}}{h'(\bar{\bar\alpha})\,\bar{\bar p} - \sin\bar{\bar\alpha}} + \frac{\bar{\bar\gamma}(1+\bar{\bar\gamma}^2)}{2\bar{\bar s}}\frac{h''(\bar{\bar\alpha})\,\bar{\bar p} - \cos\bar{\bar\alpha}}{h'(\bar{\bar\alpha})\,\bar{\bar p} - \sin\bar{\bar\alpha}} + \frac{3(1+4\bar{\bar\gamma}^2+3\bar{\bar\gamma}^4)}{4\bar{\bar s}^2} \tag{A.11}$$

Finally,

$$Y_0 = \cos\bar\alpha - g(\bar\alpha)\bar\mu, \tag{A.12}$$

$$Y_1 = \bar s\,(g(\bar\alpha) + h(\bar\alpha)\bar\mu) \tag{A.13}$$

for EP2 and

$$Y_2 = \frac{1}{2}\left[g(\bar{\bar\alpha}) + h(\bar{\bar\alpha})\bar{\bar\mu} - \bar{\bar\alpha}\bar{\bar\gamma}^2(g'(\bar{\bar\alpha}) + h'(\bar{\bar\alpha})\bar{\bar\mu})\right], \tag{A.14}$$

which is required for the EP3 Green's function.